A Generalized Gaussian Extension to the Rician Distribution for SAR Image Modeling

Oktay Karakuş, Ercan E. Kuruoglu, Alin Achim,

Abstract

In this paper, we present a novel statistical model, *the generalized-Gaussian-Rician* (GG-Rician) distribution, for the characterization of synthetic aperture radar (SAR) images. Since accurate statistical models lead to better results in applications such as target tracking, classification, or despeckling, characterizing SAR images of various scenes including urban, sea surface, or agricultural, is essential. The proposed statistical model is based on the Rician distribution to model the amplitude of a complex SAR signal, the in-phase and quadrature components of which are assumed to be generalized-Gaussian distributed. The proposed amplitude GG-Rician model is further extended to cover the intensity SAR signals. In the experimental analysis, the GG-Rician model is investigated for amplitude and intensity SAR images of various frequency bands and scenes in comparison to state-of-the-art statistical models that include $\mathcal{K}$, Weibull, Gamma, and Lognormal. In order to decide on the most suitable model, statistical significance analysis via Kullback-Leibler divergence and Kolmogorov-Smirnov statistics are performed. The results demonstrate the superior performance and flexibility of the proposed model for all frequency bands and scenes, and its applicability on both amplitude and intensity SAR images.

Index Terms

SAR amplitude modeling, SAR intensity modeling, Non-Gaussian scattering, generalized-Gaussian-Rician distribution.

I. Introduction

SYNTHETIC aperture radar (SAR) imagery is an essential source of information in the analysis of various terrains thanks to its capability to capture wider areas under different weather conditions. Statistical modeling of SAR images plays an essential role in characterizing various scenes and underpins applications such as classification [1], [2], or denoising [3], [4]. The literature abounds with numerous statistical models for different SAR scenes, which are either theoretical or empirical, and all these models have some advantages and disadvantages according to the scene and/or frequency band employed.

In this paper, we address the problem of accurately modeling the SAR amplitude/intensity data within the context of probability density function (pdf) estimation by assuming the back-scattered SAR signal components possess heavy-tailed and/or non-Gaussian nature. Specifically, we aim to propose a generic and flexible statistical model, in order to cover various different characteristics of the back-scattered SAR signal, and that will benefit applications such as despeckling, classification, or segmentation.

The standard SAR model defines the back-scattered SAR signal received by a SAR sensor as a complex signal $R = x + iy$, where x and y are the real and imaginary parts respectively, and follows several assumptions [5], [6]:

1) The number of scatterers is large,
2) The scatterers are statistically independent,
3) The instantaneous scattering phases are statistically independent of the amplitudes,
4) The phase is uniformly distributed,
5) The reflectors are relatively small when compared to the illuminated scene,
6) There is no dominating scatterer in the scene.

In particular, the first two assumptions recall the central limit theorem whereby the real and imaginary parts are jointly Gaussian. Combined with assumption 6), this leads to the case where x and y are independent and identically distributed (i.i.d.) zero-mean Gaussian random variables,

$$x \sim \mathcal{N}(0, \sigma^2) \quad \text{and} \quad y \sim \mathcal{N}(0, \sigma^2). \tag{1}$$

Thence, the amplitude distribution becomes the *Rayleigh* distribution, the probability density function (pdf) of which is given by

$$f(r|\sigma) = \frac{r}{\sigma^2} \exp\left(-\frac{r^2}{2\sigma^2}\right) \tag{2}$$

This work was supported by the UK Engineering and Physical Sciences Research Council (EPSRC) under grant EP/R009260/1 (AssenSAR).

Oktay Karakuş and Alin Achim are with the Visual Information Laboratory, University of Bristol, Bristol BS1 5DD, U.K. (e-mail: o.karakus@bristol.ac.uk; alin.achim@bristol.ac.uk)

Ercan E. Kuruoglu is with Data Science and Information Technology Center, Tsinghua-Berkeley Shenzhen Institute, China and is on leave from ISTI-CNR, Pisa, Italy. (e-mail: ercan.kuruoglu@isti.cnr.it)

where $r = \sqrt{x^2 + y^2}$ refers to the amplitude with phase $\theta = \arctan(x/y)$, and σ is the scale parameter.

In cases when the illuminated scene includes a dominating scatterer and hence assumption 6) is no longer valid, x and y become identically and independent, but this time non-zero-mean (δ) Gaussian random variables as

$$x \sim \mathcal{N}(\delta, \sigma^2) \quad \text{and} \quad y \sim \mathcal{N}(\delta, \sigma^2). \tag{3}$$

where $\delta > 0$ is the non-zero mean of components x and y [7]. Hence, the amplitude distribution follows the *Rician* distribution with pdf given by

$$f(r|\gamma, \Delta) = \frac{r}{\sigma^2} \exp\left(-\frac{r^2 + \Delta^2}{2\sigma^2}\right) \mathcal{I}_0\left(\frac{r\Delta}{\sigma^2}\right) \tag{4}$$

where Δ is the location parameter and $\mathcal{I}_0(\cdot)$ refers to the zeroth-order modified Bessel function of the first kind.

Even though they are theoretically appealing and analytically simple, Gaussian/Rayleigh based statistical models do not reflect the real life phenomena in most cases for SAR reflections. Thus, there are numerous statistical models in the literature which were developed to account for non-Rayleigh cases, and proven to be successful for modeling SAR imagery. Among those, the $\mathcal{K}$ distribution [8]–[10] is one of the important statistical models for modeling both the amplitude and intensity SAR images. The $\mathcal{K}$ distribution pdf for amplitude modeling is expressed as

$$f(r|\alpha, \gamma) = \frac{2}{\gamma\Gamma(\alpha + 1)} \left(\frac{r}{2\gamma}\right)^{\alpha+1} K_\alpha\left(\frac{r}{\gamma}\right) \tag{5}$$

where α and γ refer to the shape, and scale parameters, respectively. The Gamma distribution is another important statistical model for characterizing multi look SAR intensity images [8], [11]. It is the generalization of the exponential distribution via averaging L single-look SAR intensities, each of which are exponentially distributed. The pdf expression for the Gamma distribution is given as

$$f(\nu|L, \gamma) = \frac{(\gamma L)^L}{\Gamma(L)} \nu^{L-1} \exp\left(-\gamma L \nu\right), \tag{6}$$

where $\nu = r^2$ is the intensity SAR signal, γ is the scale parameter and $\Gamma(\cdot)$ refers to the Gamma function.

Contrary to the theoretical models discussed above, the Weibull distribution is an empirical statistical model, and has been used in the literature [10], [12], [13] to model SAR images in both amplitude and intensity formats. The Weibull pdf is expressed as

$$f(r|\alpha, \gamma) = \frac{\alpha}{\gamma} \left(\frac{r}{\gamma}\right)^{\alpha-1} \exp\left(-\left(\frac{r}{\gamma}\right)^\alpha\right) \tag{7}$$

where α refers to the shape parameter, and γ is the scale parameter. The Lognormal distribution is another empirical model like Weibull and has generally been used to model SAR amplitude images [14], [15]. The lognormal pdf expression is

$$f(r|\mu, \gamma) = \frac{1}{r\gamma\sqrt{2\pi}} \exp\left(-\frac{(\log r - \mu)^2}{2\gamma^2}\right) \tag{8}$$

where γ is the scale, and μ is the location parameter.

In a previous study, following the observation of non-Gaussian reflections in urban areas, Kuruoglu & Zerubia [5] have proposed a generalized central limit theorem based statistical model which extends the standard scattering models discussed above by considering the real and the imaginary parts of the complex back-scattered SAR signal to be jointly symmetric-α-Stable random variables. This model, called the generalized Rayleigh distribution (will be denoted as Stable-Rayleigh, or shortly SR for the rest of the paper) for amplitude SAR images, the pdf of which is given as

$$f(r|\alpha, \gamma) = r \int_0^\infty s \exp\left(-\gamma s^\alpha\right) \mathcal{J}_0(sr) ds \tag{9}$$

where α and γ refer to the shape, and scale parameters, respectively. SR has been shown to be a good choice for urban SAR image modeling in [5], [16] and successfully applied to despeckling problem in [3].

Moser et, al, [6] have proposed another generalized theoretical statistical model for amplitude SAR modeling, which is similar to SR [5], by assuming the real and imaginary parts of the back-scattered signals to be independent zero-mean generalized Gaussian (GG) random variables, which leads to the generalized Gaussian Rayleigh (GGR) distribution, with the pdf [6]

$$f(r|\alpha, \gamma) = \frac{\alpha^2 r}{4\gamma^2\Gamma^2(\frac{1}{\alpha})} \int_0^{2\pi} \exp\left(-\frac{|r\cos\theta|^\alpha + |r\sin\theta|^\alpha}{\gamma^\alpha}\right) d\theta \tag{10}$$

where α and γ refer to the shape, and scale parameters, respectively.

In a recent study [17], we have proposed a novel statistical model, namely the *Laplace-Rician* distribution for modeling amplitude SAR images of the sea surface. The Laplace-Rician model is based on the Rician distribution, whereby we assume

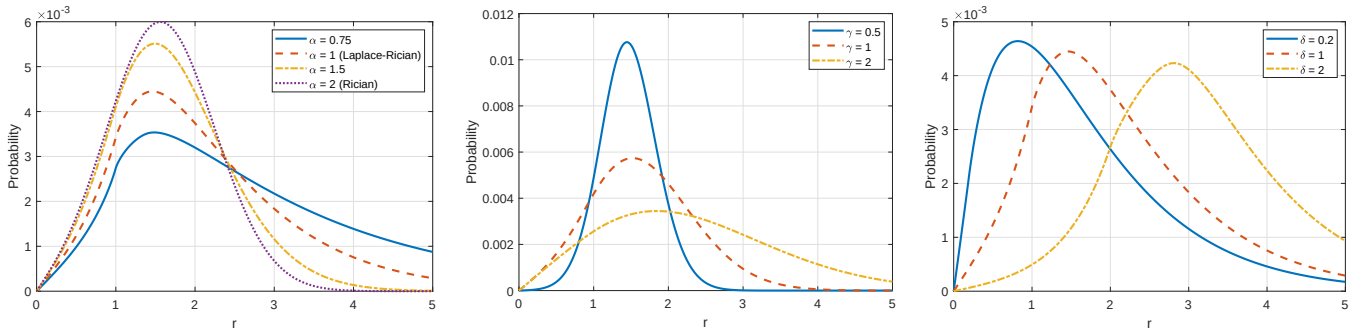

(a) (b) (c)

Fig. 1. The proposed GG-Rician distribution pdfs for different model parameters of (a) the shape parameter α ($\gamma = 1$ and $\delta = 1$), (b) the scale parameter γ ($\alpha = 1.7$ and $\delta = 1$), and (c) the location parameter δ ($\alpha = 1$ and $\gamma = 1$).

that the real and imaginary parts of the back-scattered SAR signal are non-zero mean Laplace distributed. The Rician distribution is widely used in SAR imaging applications being particularly important in characterizing SAR scenes containing many strong back-scattered echoes. These include natural targets such as forest canopy, mountain tops, sea waves, as well as some man-made structures with dihedral or trihedral configurations such as buildings, or vessels [7], [18]–[23]. Combining the Rician idea with the non-Gaussian case via the Laplace distribution in [17] addresses both the non-Rayleigh and heavy-tailed characteristics of amplitude SAR images. The Laplace-Rician model, despite being limited to a Laplace distribution as the back-scattered SAR signal components' statistical model, showed superior performance for modeling amplitude SAR images of the sea surface when compared to state-of-the-art statistical models such as Weibull, lognormal, and $\mathcal{K}$ [17].

In this paper, we propose a novel statistical model by extending the Laplace-Rician model to a much more general case, where the back-scattered SAR signal components are *non-zero mean Generalized-Gaussian* distributed. We further introduce a Markov chain Monte Carlo (MCMC) based Bayesian parameter estimation method for the proposed statistical model. We demonstrate the modeling capability of the proposed model for amplitude/intensity SAR images from satellite platforms, including TerraSAR-X, ICEYE, COSMO/Sky-Med, Sentinel-1 and ALOS2, and for illuminated scenes of urban, agricultural, land cover, sea surface with and without ships, along with several mixed scenes. We evaluate the performance of the proposed model in comparison to state-of-the-art statistical models including $\mathcal{K}$, Rayleigh, Rician, Gamma, Weibull, Lognormal, SR [5], and GGR [6].

The rest of the paper is organized as follows: we present the proposed statistical model in Section II. The Bayesian parameter estimation method is presented in Section III, whilst the experimental analysis is demonstrated in Section IV. Section V concludes the paper with remarks and future work.

II. Generalized Gaussian Rician Model

In this section, we introduce our main contribution, which is a novel statistical model derived as an extension of the generalized-Gaussian distribution into the Rician scattering idea. Our derivation starts by assuming that the illuminated SAR scene includes one (or more) dominating scatterers, such as vehicles, buildings, sea waves. Following this, the sixth assumption given above for the back-scattered SAR signal will not be valid anymore. Then, as in the Rician case, the real and imaginary components of the back-scattered complex SAR signal will be non-zero mean random variables. We now recall the generalized Gaussian pdf

$$f(x|\alpha,\gamma,\delta) = \frac{\alpha}{2\gamma\Gamma(\frac{1}{\alpha})} \exp\left(-\left|\frac{x-\delta}{\gamma}\right|^{\alpha}\right), \tag{11}$$

where δ is the location parameters. In order to have a Rayleigh-type amplitude distribution, the location parameter δ is assumed to be zero, where the assumption 6) is valid. However, for non-zero δ, as long as the complex SAR signal components x and y are independent [6], the joint pdf can be written as

$$f(x,y|\alpha,\gamma,\delta) = f(x|\alpha,\gamma,\delta) \times f(y|\alpha,\gamma,\delta) \tag{12}$$

$$= \frac{\alpha}{2\gamma\Gamma(\frac{1}{\alpha})} \exp\left(-\left|\frac{x-\delta}{\gamma}\right|^{\alpha}\right) \frac{\alpha}{2\gamma\Gamma(\frac{1}{\alpha})} \exp\left(-\left|\frac{y-\delta}{\gamma}\right|^{\alpha}\right) \tag{13}$$

$$= \frac{\alpha^2}{4\gamma^2\Gamma^2(\frac{1}{\alpha})} \exp\left(-\frac{|x-\delta|^{\alpha}+|y-\delta|^{\alpha}}{\gamma^{\alpha}}\right). \tag{14}$$

Then, the amplitude distribution can be written by using the identity, $f(r,\theta) = r f(r\cos\theta, r\sin\theta)$, as

$$f(r,\theta|\alpha,\gamma,\delta) = r\frac{\alpha^2}{4\gamma^2\Gamma^2(\frac{1}{\alpha})}\exp\left(-\frac{|r\cos\theta-\delta|^\alpha+|r\sin\theta-\delta|^\alpha}{\gamma^\alpha}\right). \tag{15}$$

Hence, the corresponding marginal amplitude pdf can be obtained by averaging (15) over θ and boils down to:

$$f(r|\alpha,\gamma,\delta) = \frac{\alpha^2 r}{4\gamma^2\Gamma^2(\frac{1}{\alpha})}\int_0^{2\pi}\exp\left(-\frac{|r\cos\theta-\delta|^\alpha+|r\sin\theta-\delta|^\alpha}{\gamma^\alpha}\right)d\theta, \tag{16}$$

The integral form pdf expression shown in (16) refers to the proposed statistical model for the amplitude distribution of a complex back-scattered SAR signal, the components of which are non-zero mean generalized-Gaussian distributed. We now state the following theorems.

Theorem 1. *The pdf expression given in (16) reduces to the Rician distribution in (4) for $\alpha = 2$, where the real and imaginary components of back-scattered SAR signal become non-zero mean Gaussian random variables.*

Proof. Starting from (16), and setting the shape parameter $\alpha = 2$, we have

$$f(r|\alpha=2,\gamma,\delta) = \frac{r}{\gamma^2\pi}\int_0^{2\pi}\exp\left(-\frac{(r\cos\theta-\delta)^2+(r\sin\theta-\delta)^2}{\gamma^2}\right)d\theta, \tag{17}$$

$$= \frac{r}{\gamma^2\pi}\int_0^{2\pi}\exp\left(-\frac{r^2-2r\delta(\cos\theta+\sin\theta)+2\delta^2}{\gamma^2}\right)d\theta, \tag{18}$$

$$= \frac{r}{\gamma^2\pi}\exp\left(-\frac{r^2+2\delta^2}{\gamma^2}\right)\int_0^{2\pi}\exp\left(\frac{r\delta(\cos\theta+\sin\theta)}{\gamma^2/2}\right)d\theta, \tag{19}$$

Using the identity

$$(\cos\theta+\sin\theta) = \sqrt{2}\cos(\theta-\pi/4), \tag{20}$$

we have

$$f(r|\gamma,\delta) = \frac{r}{\gamma^2\pi}\exp\left(-\frac{r^2+2\delta^2}{\gamma^2}\right)\int_0^{2\pi}\exp\left(\frac{r\sqrt{2}\delta\cos(\theta-\pi/4)}{\gamma^2/2}\right)d\theta. \tag{21}$$

Recall that the zeroth order modified Bessel function of the first kind is expressed as

$$\mathcal{I}_0(z) = \frac{1}{2\pi}\int_0^{2\pi}\exp(z\cos\theta)\,d\theta. \tag{22}$$

After basic manipulations we can express the pdf as

$$f(r|\gamma,\delta) = \frac{2\pi r}{\gamma^2\pi}\exp\left(-\frac{r^2+2\delta^2}{\gamma^2}\right)\underbrace{\frac{1}{2\pi}\int_0^{2\pi}\exp\left(\frac{r\sqrt{2}\delta}{\gamma^2/2}\cos(\theta-\pi/4)\right)d\theta}_{\mathcal{I}_0\left(\frac{r\sqrt{2}\delta}{\gamma^2/2}\right)}. \tag{23}$$

It is straightforward to see that the integral on the right hand side is effectively a zeroth order modified Bessel function of the first kind, and hence we have

$$f(r|\gamma,\delta) = \frac{r}{\gamma^2/2}\exp\left(-\frac{r^2+2\delta^2}{\gamma^2}\right)\mathcal{I}_0\left(\frac{r\sqrt{2}\delta}{\gamma^2/2}\right), \tag{24}$$

which is the Rician distribution for $\gamma^2/2 = \sigma^2$ and $\sqrt{2}\delta = \Delta$ in (4). □

Theorem 2. *The pdf expression given in (16) is the Laplace-Rician distribution [17] for $\alpha = 1$,*

$$f(r|\gamma,\delta) = \frac{r}{4\gamma^2}\int_0^{2\pi}\exp\left(-\frac{|r\cos\theta-\delta|+|r\sin\theta-\delta|}{\gamma}\right)d\theta. \tag{25}$$

where the real and imaginary components of back-scattered SAR signal are distributed according to a non-zero mean Laplace distribution.

Proof. For the proof of Theorem 2, we refer the reader to [17]. □

Remark 1. *We refer to the proposed pdf expression in (16) as the generalized Gaussian-Rician distribution (GG-Rician), since it extends the Rician amplitude model to a heavy-tailed form via the generalized Gaussian distributed complex SAR signal components.*

To give a feel for the characteristics of this class of distributions, they are plotted for various values of their defining parameters in Figure 1.

A. Extension to Intensity SAR Images

The derived proposed statistical model (16) characterizes the amplitude SAR signal. However, for some applications, intensity SAR images have been used instead of amplitude images. In this section, we derive the intensity pdf expression for the proposed GG-Rician statistical model.

For an intensity SAR image, the pdf expression can be calculated from the pdf of the amplitude image using the pdf transformation formula:

$$f_I(\nu) = \frac{1}{2\nu} f_A(\sqrt{\nu}) \tag{26}$$

where $\nu = r^2$ refers to the intensity with the pdf of $f_I(\cdot)$. Then, using the identity in (26), the GG-Rician intensity pdf can be written as

$$f_I(\nu|\alpha,\gamma,\delta) = \frac{\alpha^2}{8\gamma^2\Gamma^2(\frac{1}{\alpha})} \int_0^{2\pi} \exp\left(-\frac{|\sqrt{\nu}\cos\theta-\delta|^\alpha + |\sqrt{\nu}\sin\theta-\delta|^\alpha}{\gamma^\alpha}\right) d\theta. \tag{27}$$

Theorem 3. *The intensity pdf expression given in (27) simplifies to the Nakagami-Rice distribution [1], [24] for $\alpha = 2$*

$$f_I(\nu|R,\Delta) = \frac{1}{R}\exp\left(-\frac{\nu+\Delta^2}{R}\right)\mathcal{I}_0\left(\frac{\sqrt{\nu\Delta^2}}{R/2}\right) \tag{28}$$

where R is the scale and Δ is the location parameter.

Proof. We start by recalling (27), and setting the shape parameter $\alpha = 2$. Then, we have

$$f_I(\nu|\alpha=2,\gamma,\delta) = \frac{1}{2\gamma^2\pi}\int_0^{2\pi}\exp\left(-\frac{|\sqrt{\nu}\cos\theta-\delta|^2+|\sqrt{\nu}\sin\theta-\delta|^\alpha}{\gamma^2}\right)d\theta, \tag{29}$$

$$= \frac{1}{2\gamma^2\pi}\int_0^{2\pi}\exp\left(-\frac{\nu-2\sqrt{\nu}\delta(\cos\theta+\sin\theta)+2\delta^2}{\gamma^2}\right)d\theta, \tag{30}$$

$$= \frac{1}{2\gamma^2\pi}\exp\left(-\frac{\nu+2\delta^2}{\gamma^2}\right)\int_0^{2\pi}\exp\left(\frac{\sqrt{\nu}\delta(\cos\theta+\sin\theta)}{\gamma^2/2}\right)d\theta. \tag{31}$$

In a way akin to the proof of Theorem 1, we can easily write the expression in (31) as

$$f_I(\nu|\gamma,\delta) = \frac{2\pi}{2\gamma^2\pi}\exp\left(-\frac{\nu+2\delta^2}{\gamma^2}\right)\underbrace{\frac{1}{2\pi}\int_0^{2\pi}\exp\left(\frac{\sqrt{\nu 2\delta^2}}{\gamma^2/2}\cos(\theta-\pi/4)\right)d\theta}_{\mathcal{I}_0\left(\frac{\sqrt{\nu2\delta^2}}{\gamma^2/2}\right)}. \tag{32}$$

It is straightforward to see that the integral on the right hand side is a zeroth order modified Bessel function of the first kind. Then, we have

$$f_I(\nu|\gamma,\delta) = \frac{1}{\gamma^2}\exp\left(-\frac{\nu+2\delta^2}{\gamma^2}\right)\mathcal{I}_0\left(\frac{\sqrt{\nu2\delta^2}}{\gamma^2/2}\right), \tag{33}$$

which is the Nakagami-Rician distribution for $\gamma^2 = R$ and $2\delta^2 = \Delta^2$, and completes the proof. □

Remark 2. *It is straightforward to observe that for $\alpha = 2$ and $\delta = 0$, with a derivation akin to Theorem 3, the corresponding intensity pdf will boil down to the **exponential distribution**, and similarly for L-look case to the **Gamma distribution**.*

As mentioned up to this point, the GG-Rician statistical model is a general statistical model, which covers various important amplitude and intensity statistical models as special members. For completeness, we provide GG-Rician pdf expressions, and some special cases in Table I.

III. Bayesian Parameter Estimation Method

Since the pdf expression in (16) is not in a compact analytical form and it does not seem to be possible to invert it to obtain parameter values, we employ a Bayesian sampling methodology in order to estimate model parameters. In this section, a Markov chain Monte Carlo (MCMC) based method is developed for estimating GG-Rician distribution parameters, namely the shape parameter α, the scale parameter γ, and the location parameter δ. In particular, the method uses the Metropolis-Hastings (MH) algorithm, and in each iteration, it applies one of three different moves:

1) $\mathcal{M}_1$ which updates δ for fixed α and γ,
2) $\mathcal{M}_2$ which updates γ for fixed α and δ,
3) $\mathcal{M}_3$ which updates α for fixed γ and δ.

TABLE I
GG-RICIAN FAMILY SPECIAL MEMBERS FOR AMPLITUDE AND INTENSITY.

Distribution	Expression
GG-Rician (Amplitude)	$f(r\|\alpha,\gamma,\delta)$ in (16)
Rayleigh	$f(r\|2,\gamma,0)$
Rician	$f(r\|2,\gamma,\delta)$
GGR [6]	$f(r\|\alpha,\gamma,0)$
Nakagami	L-look average of $f(r\|2,\gamma,0)$
Laplace-Rician [17]	$f(r\|1,\gamma,\delta)$
GG-Rician (Intensity)	$f_I(\nu\|\alpha,\gamma,\delta)$ in (27)
Exponential	$f_I(\nu\|2,\gamma,0)$
Nakagami-Rice	$f_I(\nu\|2,\gamma,\delta)$
Gamma	L-look average of $f_I(\nu\|2,\gamma,0)$

The proposed parameter estimation procedure is given in Algorithm 1. Given the observed data y, the hierarchical model is expressed by Bayes' theorem as

$$p(\alpha,\delta,\gamma|y) \propto p(y|\alpha,\delta,\gamma)p(\alpha)p(\gamma)p(\delta) \tag{34}$$

where $p(\alpha,\delta,\gamma|y)$ is the joint posterior distribution, or the MH target distribution, $p(y|\alpha,\delta,\gamma)$ refers to the likelihood distribution, and $p(\alpha)$, $p(\gamma)$ and $p(\delta)$ are the priors.

Due to lack of knowledge on conjugate priors, we choose non-informative priors for the shape, location and scale (Jeffrey's) parameters. In particular, we assume that the location and shape parameters α and δ are uniformly distributed and that the prior for the scale parameter γ is $p(\gamma) = 1/\gamma$, which leads to $p(\alpha,\delta,\gamma) \sim 1/\gamma$. The likelihood $p(y|\alpha,\delta,\gamma)$ is the GG-Rician distribution in (16) with parameters α, γ and δ.

Depending on the selected move in iteration i, one of the proposal distributions given below is used to sample candidate parameters δ^*, γ^* or α^*

$$\mathcal{M}_1: \quad \delta^* \propto q\left(\delta^*|\delta^{(i)}\right) = \mathcal{U}\left(\delta^{(i)}-\epsilon, \delta^{(i)}+\epsilon\right), \tag{35}$$

$$\mathcal{M}_2: \quad \gamma^* \propto q\left(\gamma^*|\gamma^{(i)}\right) = \mathcal{N}\left(\gamma^{(i)}, \xi^2\right), \tag{36}$$

$$\mathcal{M}_3: \quad \alpha^* \propto q\left(\alpha^*|\alpha^{(i)}\right) = \mathcal{U}\left(\alpha^{(i)}-\eta, \alpha^{(i)}+\eta\right), \tag{37}$$

where $\mathcal{U}(\cdot)$ is the uniform, and $\mathcal{N}(\cdot)$ is the Gaussian distributions, both of which are defined in the interval $[0,\infty]$ since α, δ and γ are positive parameters. η, ϵ and ξ are hyper-parameters of the proposal distributions. Please note that these selection of proposals are not unique and can be replaced with any other distribution for better performance in estimating model parameters, faster convergence, etc.

Consequently, the acceptance probability expressions for each move can be expressed as

$$A_{\mathcal{M}_1} = \min\left(1, \frac{p(y|\alpha^*,\delta^*,\gamma^*)q\left(\delta^{(i)}|\delta^*\right)}{p(y|\alpha^{(i)},\delta^{(i)},\gamma^{(i)})q\left(\delta^*|\delta^{(i)}\right)}\right), \tag{38}$$

$$A_{\mathcal{M}_2} = \min\left(1, \frac{p(y|\alpha^*,\delta^*,\gamma^*)p(\gamma^*)q\left(\gamma^{(i)}|\gamma^*\right)}{p(y|\alpha^{(i)},\delta^{(i)},\gamma^{(i)})p(\gamma^{(i)})q\left(\gamma^*|\gamma^{(i)}\right)}\right), \tag{39}$$

$$A_{\mathcal{M}_3} = \min\left(1, \frac{p(y|\alpha^*,\delta^*,\gamma^*)q\left(\alpha^{(i)}|\alpha^*\right)}{p(y|\alpha^{(i)},\delta^{(i)},\gamma^{(i)})q\left(\alpha^*|\alpha^{(i)}\right)}\right). \tag{40}$$

IV. EXPERIMENTAL ANALYSIS

The proposed method was tested from four different perspectives using both simulated and real data.

1) In the first simulation case, we used synthetically generated GG-Rician data for various parameters and tested the parameter estimation performance of the proposed MCMC method.
2) Second, we subsequently conducted experiments to determine the best fitting amplitude distribution for given real SAR images of various scenes.
3) Third, we evaluated the estimated GG-Rician model parameters on a large SAR scene, which was then decomposed into several image patches of 250×250. For each patch, estimated model parameters are combined to create a parameter

map, which potentially gives ideas on how the different parts of a large image affects the estimated parameters of the GG-Rician model.

4) For the fourth and the last set of simulations, we performed a modeling study on intensity SAR images using the GG-Rician distribution.

Algorithm 1 MCMC Parameter Estimation for GG-Rician Distribution

Inputs: Given data y.
Output: Joint Posterior $f(\alpha, \delta, \gamma|y)$
Initialize: $\alpha^{(1)}$, $\delta^{(1)}$, $\gamma^{(1)}$, η, ν and ξ.
for $i = 1 : N_{iter}$ **do**
  Choose Move, $m^{(i)}$ equally likely between $\mathcal{M}_1$, $\mathcal{M}_2$ or $\mathcal{M}_3$
  if $m^{(i)} \rightarrow \mathcal{M}_1$ **then**
    Sample $\delta^* \sim q\left(\delta^*|\delta^{(i)}\right)$
    Set $\alpha^* = \alpha^{(i)}$ and $\gamma^* = \gamma^{(i)}$ and $A = A_{\mathcal{M}_1}$.
  elseif $m^{(i)} \rightarrow \mathcal{M}_2$ **then**
    Sample $\gamma^* \sim q\left(\gamma^*|\gamma^{(i)}\right)$
    Set $\alpha^* = \alpha^{(i)}$ and $\delta^* = \delta^{(i)}$ and $A = A_{\mathcal{M}_2}$.
  elseif $m^{(i)} \rightarrow \mathcal{M}_3$ **then**
    Sample $\alpha^* \sim q\left(\alpha^*|\alpha^{(i)}\right)$
    Set $\delta^* = \delta^{(i)}$ and $\gamma^* = \gamma^{(i)}$ and $A = A_{\mathcal{M}_3}$.
  end if
  Sample random variable $u \sim \mathcal{U}(0, 1)$
  if $u \leq A$ **then**
    $\alpha^{(i+1)} = \alpha^*$ and $\delta^{(i+1)} = \delta^*$ and $\gamma^{(i+1)} = \gamma^*$
  else
    $\alpha^{(i+1)} = \alpha^{(i)}$ and $\delta^{(i+1)} = \delta^{(i)}$ and $\gamma^{(i+1)} = \gamma^{(i)}$
  end if
end for

TABLE II
MODELING AND STATISTICAL SIGNIFICANCE RESULTS FOR SYNTHETICALLY GENERATED GG-RICIAN DATA SETS.

(α, δ, γ)	**Est. Shape*** $(\hat{\alpha})$	**Est. Location*** $(\hat{\delta})$	**Est. Scale*** $(\hat{\gamma})$	**KL Div.**	**KS Score**
(1.7. 2.9, 2.3)	1.58±0.111	2.74±0.040	2.26±0.129	0.0043	0.0194
(1.45, 1, 5)	1.42±0.081	1.09±0.391	4.97±0.342	0.0049	0.0158
(1.1, 10, 2)	1.04±0.043	10.09±0.051	1.86±0.118	0.0069	0.0112
(0.7, 5, 1.5)	0.79±0.022	4.86±0.091	1.98±0.133	0.0137	0.0321
(1.2, 47, 32)	1.31±0.078	46.74±0.787	34.92±2.207	0.0042	0.0191
(0.5, 2, 0.5)	0.59±0.032	2.00±0.086	0.94±0.186	0.0153	0.0468
(1, 1.7, 1.3)	1.04±0.038	1.71±0.035	1.39±0.081	0.0018	0.0134
(2, 2, 4)	1.85±0.151	2.05±0.163	3.73±0.242	0.0032	0.0079

* Estimated values are given in a format of: (*posterior mean*)±(*posterior standard deviation*).

We used the statistical significance measures of *Kullback-Leibler* (KL) divergence, *Kolmogorov-Simirnov* (KS) score in order to assess the performance of fitting distributions. Smaller KL and KS values indicate a better modeling performance. KL divergence is used to test the performance by considering the estimated pdfs and data histograms, whereas KS score is calculated by evaluating the estimated and the empirical cumulative distribution functions (CDFs).

The number of iterations, N_{iter} in the MCMC parameter estimation method was set to 1000 and the first 500 iterations were discarded as burn-in period. Initial values for the parameters $\alpha^{(1)}$, $\delta^{(1)}$ and $\gamma^{(1)}$ were set to 2, 10 and 10, respectively. For proposal hyper-parameters, we chose $\epsilon = 2.5$, $\xi = 3$, and $\eta = 0.5$ after a trial-error procedure. All three model moves $\mathcal{M}_1$, $\mathcal{M}_2$ and $\mathcal{M}_3$ are equiprobable whilst satisfying $p(\mathcal{M}_1) + p(\mathcal{M}_2) + p(\mathcal{M}_3) = 1$. For all state-of-the-art statistical models, we utilized an MCMC based maximum likelihood (ML) methodology to estimate the model parameters. The number of histogram bins for analysis was calculated for each image by using Sturge's method [25].

A. Synthetically Generated Data

In the first set of simulations, eight synthetically generated GG-Rician data sets were obtained and the proposed parameter estimation method was used to estimate α, δ and γ for each data set. The corresponding data sets were generated for (α, δ, γ) which are given in Table II. Each data set has 1500 samples, and the results are presented in Table II and Figure 2.

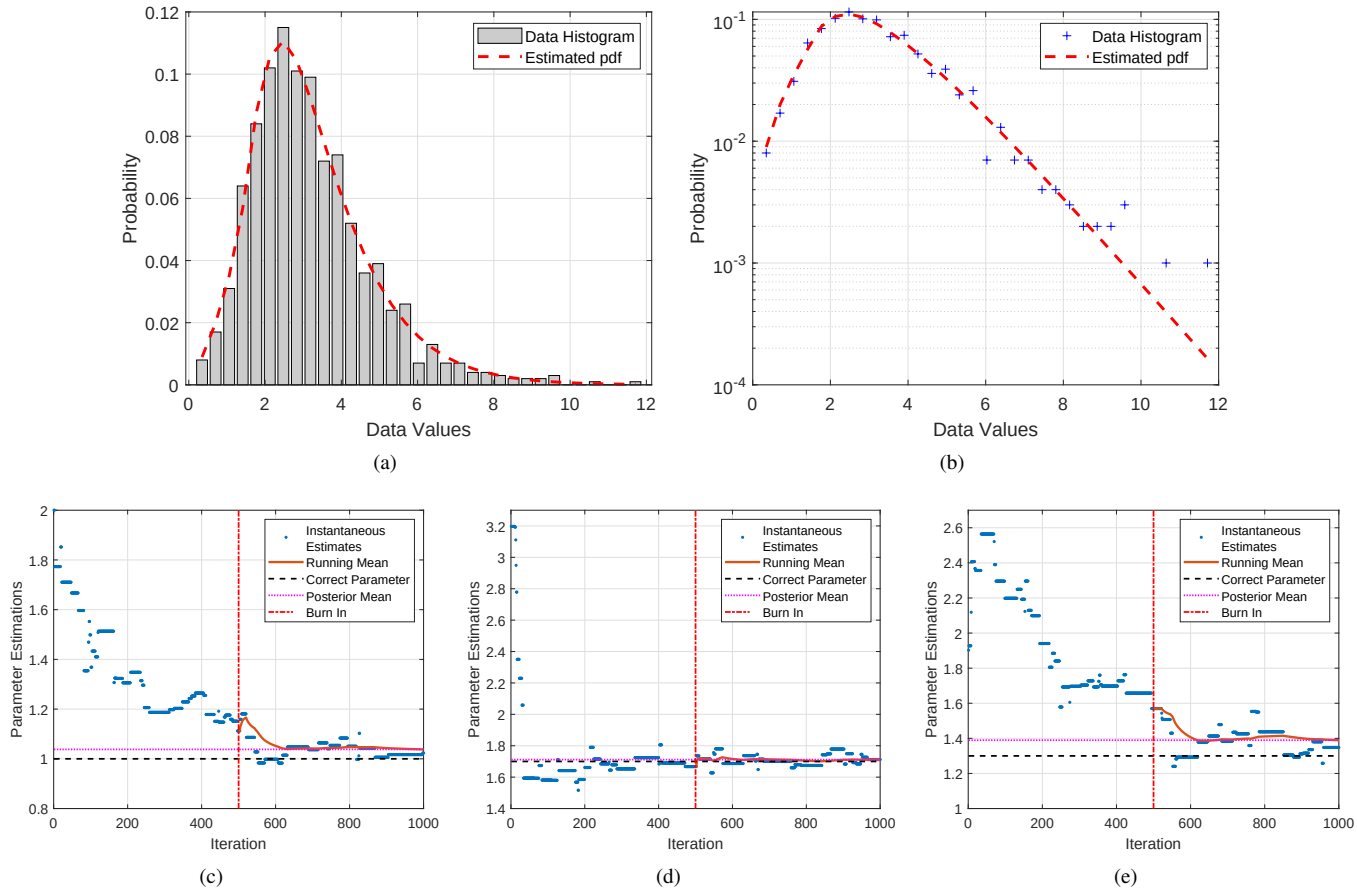

Fig. 2. Modeling and parameter estimation results for synthetically generated data for the GG-Rician model of (1, 1.7, 1.3). (a) pdf Fitting. (b) Log-pdf fitting. Instantaneous estimates are presented for (c) The shape parameter α, (d) The location parameter δ, and (e) The scale parameter γ.

By examining estimated values in Table II, we can clearly see that all the model parameters α, γ and δ are correctly estimated and are very close to their true values. For all eight example data sets, statistical significance values are obviously low which certifies that the model parameters are successfully estimated.

Figure 2 shows modeling and parameter estimation results for the synthetically generated data from GG-Rician model of (1, 1.7, 1.3). When examining sub-figures in Figure 2-(a) and (b), we can obviously state that the fitted distribution follows the generated data histogram well for both numerical and logarithmic scales. Sub-figures in Figure 2-(c)-(e) show instantaneous estimates for the parameters α, δ and γ, respectively. The vertical line in all sub-figures represent the burn-in period, whilst the black and pink lines refer to the true and posterior mean values of the model parameters. When examining sub-figures in Figure 2-(c)-(e), we can clearly state that the parameter estimation method converges to the true parameter values within N_{iter} iterations. Furthermore, 500 iterations of burn-in period looks like a good choice since all instantaneous estimates are scattered near the true model parameters after the burn-in period.

B. Real Amplitude SAR Data

In the second set of simulations, the proposed method was tested for 43 different SAR images coming from various platforms with frequency bands of *X* (TerraSAR-X, COSMO-SkyMed and ICEYE), *L* (ALOS-2) and *C* (Sentinel-1). Each SAR image corresponds to one type of scene investigate, i.e. *urban, agricultural, mountain, land cover, mixed* and *sea surface with and without ships and their wakes*. Since we have three sources for X band SAR imagery as mentioned above, we have more X band example images in this study, the exact distribution of images in terms of scenes and frequency bands is given in Table III.

Initially, each utilized SAR image was down-sampled to have a sample size of around 8000-10000. The down-sampling factor was different for each image since images had various sizes. The modeling performance of the proposed statistical model was compared to state-of-the-art statistical models including $\mathcal{K}$, Rayleigh, Rician, Weibull, lognormal, SR [5] and GGR [6]. Finally, the corresponding modeling results are presented in Tables IV to VII, and depicted in Figure 3. In Tables IV and V, to prevent repeating similar results and conclusions, instead of sharing KL and KS values specifically for each image, we shared

TABLE III
DISTRIBUTION OF IMAGES IN TERMS OF SCENE AND FREQUENCY BANDS.

Scene	Frequency band			Total
	X	C	L	
Urban	4	3	0	7
Agricultural	3	3	2	8
Land	4	1	1	6
Mountain	1	2	3	6
wS/Sea	3	1	1	5
woS/Sea	2	2	1	5
Mixed	2	3	1	6
Total	19	15	9	43

the percentages of images for which the models achieved the best performance in terms of KL or KS for various SAR scenes. Tables VI and VII present the same performance analysis for different SAR frequency bands.

Modeling results in terms of KL divergence and KS score for all 43 SAR images utilized in this paper are presented in the first rows of Tables IV and V, respectively. This statistical significance analysis clearly shows that for around 60% and 81% of the images respectively for KL and KS scores, the most suitable distribution to model SAR amplitude images of different scenes is the proposed GG-Rician distribution. When examining the scene specific statistical significance results in terms of KL divergence in Table IV, we can obviously state that for each of the utilized SAR scenes, the GG-Rician model achieves the best performance results by being most suitable model for more (or at least equal number of) images than the second best statistical model. On the other hand, Lognormal model also shows a good modeling performance for urban and mountain scenes by achieving the best results for the same number of images as the proposed model in terms of KL divergence. For the scene specific KS scores presented in Table V, for all the scenes utilized in this paper, the GG-Rician model achieves the smallest KS Score values for more images than the second best model, which makes the GG-Rician achieve the best modeling results.

When we specifically examine the frequency band performance in terms of KL divergence given in Table VI, For X and C band SAR amplitude images, the GG-Rician model shows the best modeling performance for most of the images, whereas for L band, Lognormal appears to be the best model over all scenes. For the KS score results presented in Table VII, for all the frequency bands, the GG-Rician appears the most suitable statistical model.

Figure 3 presents SAR images for six different scenes and their modeling results in logarithmic scale. The log-scale pdf modeling results in Figure 3 confirm the numerical results presented in Tables IV to VII, whereby the GG-Rician model outperforms most of the reference models utilized in this study and follows the data histograms better than the others.

In all the statistical significance results presented in Tables IV to VII, despite being the best model over all images, it can be clearly seen that KL divergence results for the GG-Rician model is somehow worse than that of KS scores. In order to analyze the reason behind this performance, we show two examples in Figure 4. The example comparison plot in Figure 4-(a) shows a modeling case where the Lognormal model achieves the best modeling results in terms of KL divergence values, whilst for the KS score the GG-Rician model is the best statistical model. Figure 4-(b) shows a modeling case where the GG-Rician model achieves the best modeling results in terms of the both statistical measures. When examining Figure 4-(a), for the data points in the rectangle, GG-Rician fails to follow the data points where Lognormal shows a closer fit. The main reason for GG-Rician model to have worse modeling results in terms of KL values is the limited amount of low amplitude pixels as shown in the example, hence the estimate being rough. Despite its worse fit for the left (lower amplitude pixels) tail of the data histogram, GG-Rician provides a better model for the data values around the peak value (high probability region in ellipse) and the right tail (higher amplitude pixels). Since KL scales the weights according to the relative entropy while KS looks at the cumulative distribution, these low amplitude areas with small number of pixels seem to have affected the results unevenly.

In order to give an example to support this reasoning and counter the average KL results, we depict the Figure 4-(b). We can clearly state that when compared to the SAR data in Figure 4-(a), data has higher probabilities for dark (low-amplitude) pixels than the bright (high-amplitude) ones, which is better described by the GG-Rician model in both tails and the main lobe. However, we can clearly see that the Lognormal model fails to model both tails and the higher probability region at the same time. This characteristic of the proposed GG-Rician model provides the reason why the proposed model is having difficulties to have lower KL divergence values for the urban and the mountain scenes (see Table IV), which are generally bright and obtain less darker radar returns. Finally, the same effects as in Figure 4-(a) and (b) can also be seen in Figure 3-(d) and (f), respectively.

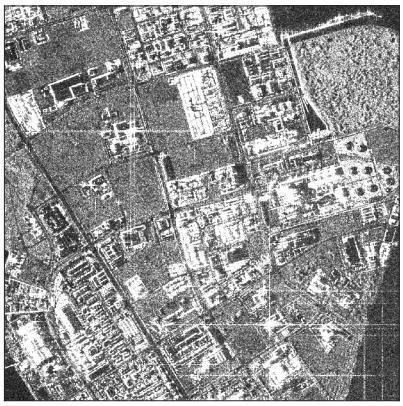

(a) Urban (X) - COSMO/Sky-Med

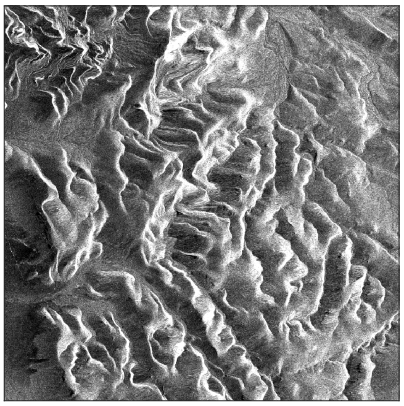

(b) Mountain (X) - ICEYE

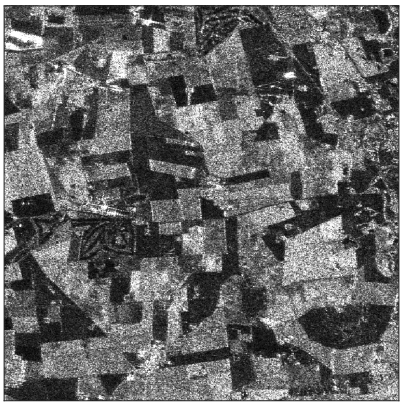

(c) Agricultural (L) - ALOS2

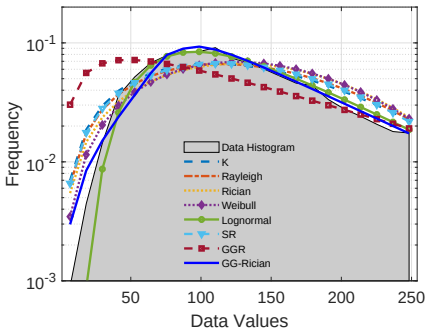

(d) Urban-logpdf

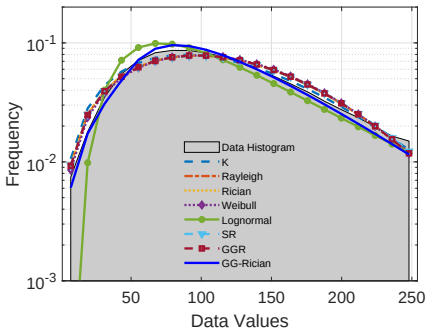

(e) Mountain-logpdf

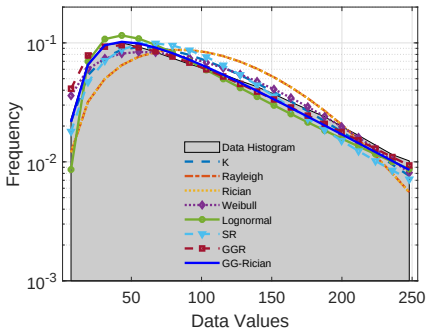

(f) Agricultural-logpdf

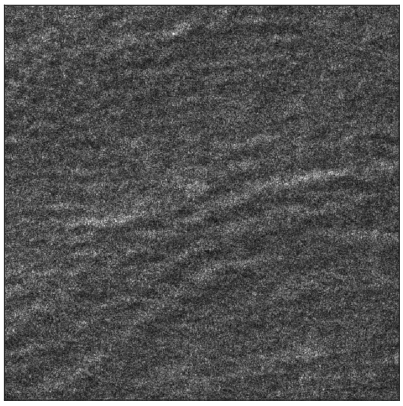

(g) Sea / woShips (X) - TerraSAR-X

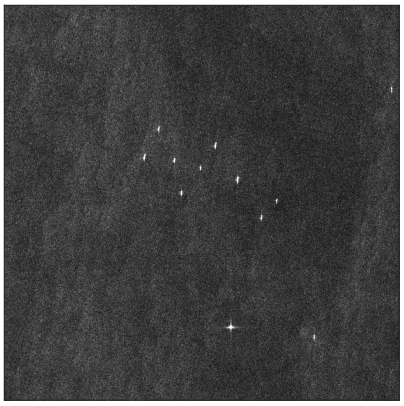

(h) Sea / wShips (C) - Sentinel-1

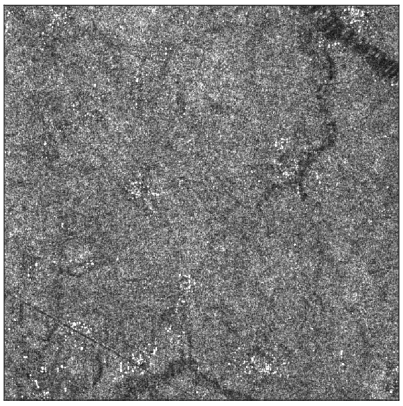

(i) Land (C) - Sentinel-1

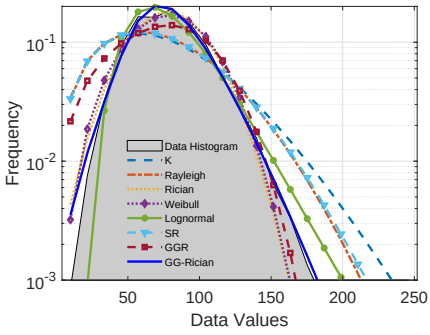

(j) Sea / woShips-logpdf

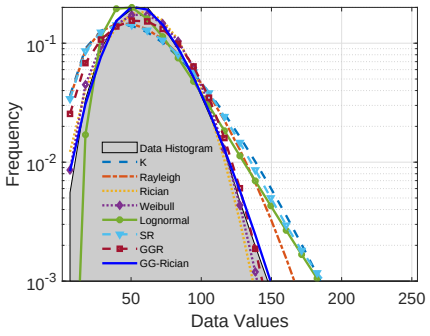

(k) Sea / wShips-logpdf

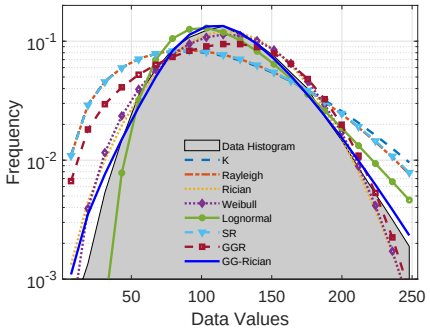

(l) Land-logpdf

Fig. 3. Visual evaluation of SAR amplitude models.

TABLE IV
MODELING PERFORMANCE PERCENTAGES IN TERMS OF KL DIVERGENCE FOR DIFFERENT SAR SCENES.

	$\mathcal{K}$	Rayleigh	Rician	Weibull	Lognormal	GGR	SR	GG-Rician
Overall	0.00%	0.00%	0.00%	4.65%	34.88%	0.00%	0.00%	**60.47%**
Urban	0.00%	0.00%	0.00%	14.29%	**42.86%**	0.00%	0.00%	**42.86%**
Agricultural	0.00%	0.00%	0.00%	0.00%	37.50%	0.00%	0.00%	**62.50%**
Mountain	0.00%	0.00%	0.00%	0.00%	**50.00%**	0.00%	0.00%	**50.00%**
Land	0.00%	0.00%	0.00%	16.67%	33.33%	0.00%	0.00%	**50.00%**
Mixed	0.00%	0.00%	0.00%	0.00%	16.67%	0.00%	0.00%	**83.33%**
wS/Sea	0.00%	0.00%	0.00%	0.00%	40.00%	0.00%	0.00%	**60.00%**
woS/Sea	0.00%	0.00%	0.00%	0.00%	20.00%	0.00%	0.00%	**80.00%**

TABLE V
MODELING PERFORMANCE PERCENTAGES IN TERMS OF KS SCORE FOR DIFFERENT SAR SCENES.

	$\mathcal{K}$	Rayleigh	Rician	Weibull	Lognormal	GGR	SR	GG-Rician
Overall	2.33%	0.00%	0.00%	6.98%	11.63%	0.00%	0.00%	**81.40%**
Urban	0.00%	0.00%	0.00%	14.29%	28.57%	0.00%	0.00%	**71.43%**
Agricultural	12.50%	0.00%	0.00%	0.00%	12.50%	0.00%	0.00%	**75.00%**
Mountain	0.00%	0.00%	0.00%	0.00%	16.67%	0.00%	0.00%	**83.33%**
Land	0.00%	0.00%	0.00%	33.33%	0.00%	0.00%	0.00%	**66.67%**
Mixed	0.00%	0.00%	0.00%	0.00%	0.00%	0.00%	0.00%	**100.00%**
wS/Sea	0.00%	0.00%	0.00%	0.00%	20.00%	0.00%	0.00%	**80.00%**
woS/Sea	0.00%	0.00%	0.00%	0.00%	0.00%	0.00%	0.00%	**100.00%**

TABLE VI
MODELING PERFORMANCE PERCENTAGES IN TERMS OF KL DIVERGENCE FOR DIFFERENT SAR FREQUENCY BANDS.

	$\mathcal{K}$	Rayleigh	Rician	Weibull	Lognormal	GGR	SR	GG-Rician
Overall	0.00%	0.00%	0.00%	4.65%	34.88%	0.00%	0.00%	**60.47%**
X	0.00%	0.00%	0.00%	10.53%	31.58%	0.00%	0.00%	**57.89%**
C	0.00%	0.00%	0.00%	0.00%	26.67%	0.00%	0.00%	**73.33%**
L	0.00%	0.00%	0.00%	0.00%	**55.56%**	0.00%	0.00%	44.44%

TABLE VII
MODELING PERFORMANCE PERCENTAGES IN TERMS OF KS SCORE FOR DIFFERENT SAR FREQUENCY BANDS.

	$\mathcal{K}$	Rayleigh	Rician	Weibull	Lognormal	GGR	SR	GG-Rician
Overall	2.33%	0.00%	0.00%	6.98%	11.63%	0.00%	0.00%	**81.40%**
X	5.26%	0.00%	0.00%	15.79%	5.26%	0.00%	0.00%	**73.68%**
C	0.00%	0.00%	0.00%	0.00%	20.00%	0.00%	0.00%	**86.67%**
L	0.00%	0.00%	0.00%	0.00%	11.11%	0.00%	0.00%	**88.89%**

C. Analysis of Estimated GG-Rician Model Parameters

In the third set of simulations, we analyzed estimated GG-Rician model parameters, and their variations depending on the different surface characteristics in a single large SAR scene.

We chose two example amplitude SAR images, each of which are TerraSAR-X products for sea surface with and without ships, and their corresponding wakes (Figure 5-(a) and (b)). We believe that SAR images of this type include several distinct structures, such as land/mountain, urban area, sea, ships, shorelines, some islands, and even agricultural, which are suitable for the analysis in this simulation case. Each large image were decomposed into 250×250 pixel patches and each patch was modeled via the proposed GG-Rician model. For each patch, we estimated model parameters and we plot them as images in Figure 5-(c)-(h).

When examining shape parameter estimations for both images, we could state that areas including bright radar returns such as mountain tops, buildings, have relatively high shape parameter estimates, e.g. around α estimates of 2-3. For the sea surface, we can conclude that the shape parameter estimates do not directly reflect the changes of the sea surface, the estimated values

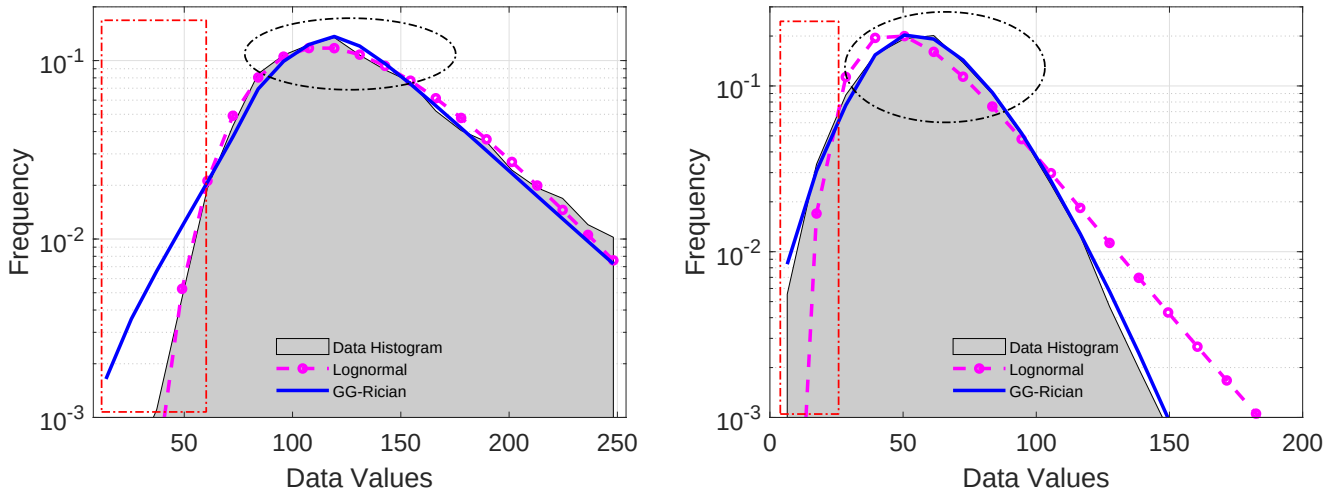

Fig. 4. A direct comparison between the GG-Rician and Lognormal models for two different cases. (a) The best in terms of KL Div. is Lognormal, whilst in terms of KS, GG-Rician is the best model. (b) GG-Rician is the best for KL and KS measures.

of which generally lie around 1-2.

In Figures 5-(d) and (g), we show the estimated location parameter, δ, for two example images. When examining these sub-figures, we can obviously state that the location parameter estimates reflect a direct relation with the original image amplitude values, and provide a so-called good "down-sampled version" of the original image. Different wave heights, shore-lines, as well as bright amplitudes such as urban areas are clearly distinguishable. We believe that as a feature, the location parameter δ of the proposed model would play an important role in classification tasks involving amplitude SAR images.

The estimated scale parameters for each patch are depicted in Figure 5-(e) and (h). Both sub-figures generally show similar characteristics to the shape parameter estimates. For bright radar returns, it takes a γ of around 100-140. The sea and land regions can be easily distinguished between them according to the estimated scale parameter value, whilst the sea surface changes are not distinguishable from the γ estimates.

Please note that, different from most of the statistical models, the GG-Rician model includes a location parameter. As a remark of this analysis, we can state that it is the most suitable parameter to reflect the radical changes on the SAR scene, and can be shown as an important advantage of the proposed statistical model, specifically in applications such as segmentation and classification.

D. Real Intensity SAR Data

In the fourth and last simulation experiment, we evaluated the performance of the intensity GG-Rician model. For this simulation, we only utilized three example intensity SAR images. We left the further analysis of the intensity model as future work.

The same procedure as for the amplitude SAR modeling was also applied here for intensity images. The same parameter estimation methodology was used to estimate the model parameters of the intensity GG-Rician model. For the reference models, in addition to $\mathcal{K}$ and Weibull (thanks to their intensity modeling capabilities), the Gamma distribution was also used.

TABLE VIII
STATISTICAL SIGNIFICANCE FOR INTENSITY SAR IMAGE MODELING

Image	Stats	$\mathcal{K}$	Weibull	Gamma	GG-Rician
wS/Sea	KL Div	0.0767	0.0756	**0.0133**	0.0154
	KS Score	0.0690	0.0564	0.0301	**0.0181**
Mixed	KL Div	0.0358	0.0755	0.0365	**0.0064**
	KS Score	0.0740	0.0867	0.0697	**0.0297**
Urban	KL Div	0.5484	0.1084	0.1622	**0.0144**
	KS Score	0.3383	0.1715	0.2117	**0.0512**

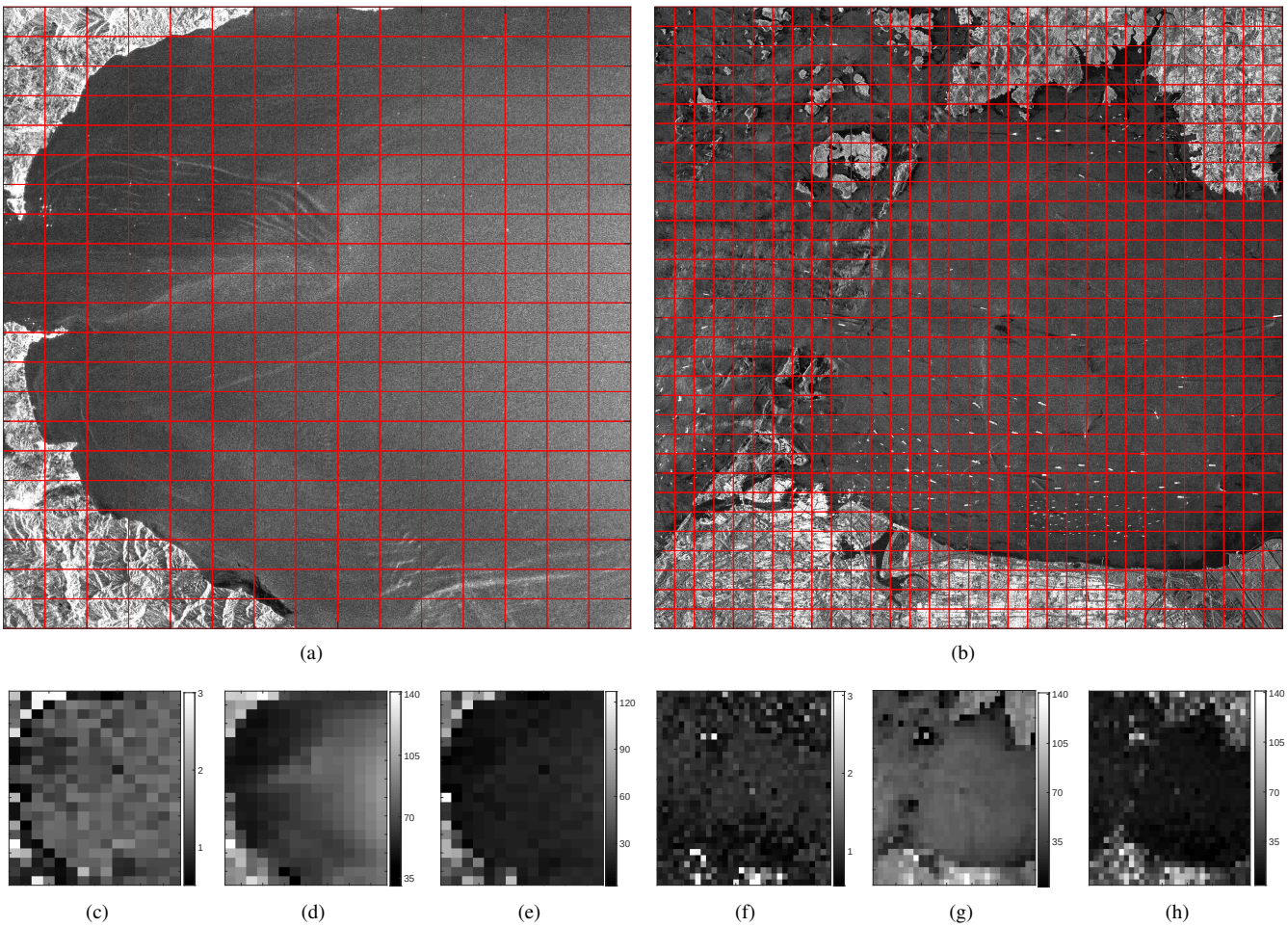

Fig. 5. Estimated model parameters for two large SAR scenes for 250×250 image patches in red rectangles. (a) Original Image-1 (5250×3750). (b) Original Image-2 (8000×8000). (c) and (f) The shape parameter α. (d) and (g) The location parameter δ. (e) and (h) The scale parameter γ.

The corresponding results are depicted in Figure 6, and statistical significance of modeling is given in Table VIII. There are three SAR images of scenes: Sea with ships, Mixed and Urban, respectively in Figure 6-(a), (b) and (c). The corresponding modeling results are presented in logarithmic scale in sub-figures from (d) to (f). The superior modeling performance of the proposed GG-Rician intensity model compared to the state-of-the-art models is obvious.

V. Conclusions

In this paper, we proposed a novel parametric statistical model, namely the GG-Rician distribution, to characterize the amplitude and the intensity of the complex back-scattered SAR signal. Specifically, the GG-Rician model is an extension of Rician model whereby the Gaussian components of the complex SAR signal are replaced by the generalized-Gaussian distribution. A closed form pdf expression in integral form was derived and a Bayesian sampling scheme for the model parameter estimation was developed. We have tested the modeling performance of the GG-Rician model both for synthetically generated and real SAR data, which are specifically coming from satellite platforms of TerraSAR-X, Sentinel-1, ICEYE, COSMO/Sky-Med and ALOS2.

The performance of the proposed statistical model was then compared to the state-of-the-art statistical models of $\mathcal{K}$, Rician, Rayleigh, Weibull, Lognormal, SR, GGR and Gamma. The results demonstrate that the proposed method achieves the best modeling results for most of the images, and outperforms state-of-the-art models for images from various frequency bands and sources. It is interesting to note that the results show the need for combining the advantages of non-Gaussian heavy-tailed modeling and non-zero mean reflections modeling provided by the Rician model. That is quite obvious when we compare Laplace-Rician with $\mathcal{K}$, SR, GGR, Rician and Rayleigh directly. Furthermore, using non-zero reflections along with the heavy-tailed modeling of the GG-Rician model shows important success in all types of SAR scenes and frequency bands.

All the experimental analyses in this paper demonstrate that the extension from Rayleigh (zero-mean components) to Rician (non-zero mean components) offers clear advantages over the Rayleigh-based GGR in [6]. On the other hand, since the GGR model is actually a simplified special member (for $\delta = 0$) of the proposed GG-Rician model, we conclude that we generalized

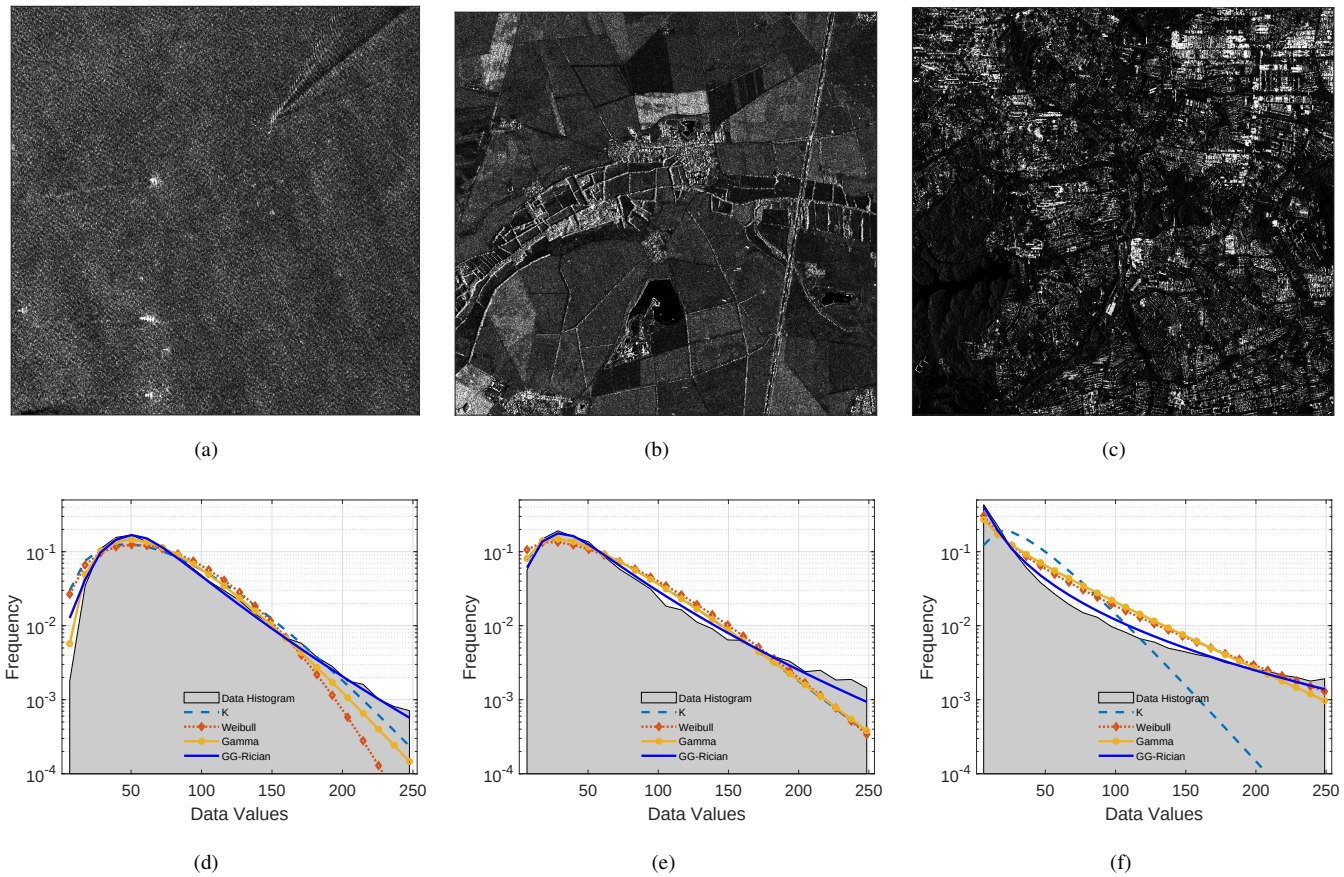

Fig. 6. Intensity modeling comparison. Intensity SAR images from scenes of (a) sea with ships, (b) mixed, and (c) urban . Sub-figures in (d)-(f) refer to the corresponding modeling results in log-pdf scale for intensity images in (a)-(c), respectively.

GGR to a more flexible and robust model that covers various characteristics.The flexibility of adjusting distribution tails (via a shape parameter) in conjunction with the location parameter demonstrates a remarkable gain over the Rician model for all the simulation scenarios considered in this paper. Some of our future work we will investigate more efficient parameter estimation methods.

ACKNOWLEDGMENT

We are grateful to the UK Satellite Applications Catapult for providing us the COSMO-SkyMed data sets employed in this study.

REFERENCES

[1] C. Tison, J.-M. Nicolas, F. Tupin, and H. Maître, "A new statistical model for Markovian classification of urban areas in high-resolution SAR images," *IEEE transactions on Geoscience and Remote Sensing*, vol. 42, no. 10, pp. 2046–2057, 2004.

[2] M. E. Mejail, J. C. Jacobo-Berlles, A. C. Frery, and O. H. Bustos, "Classification of SAR images using a general and tractable multiplicative model," *International Journal of Remote Sensing*, vol. 24, no. 18, pp. 3565–3582, 2003.

[3] A. Achim, E. E. Kuruoglu, and J. Zerubia, "SAR image filtering based on the heavy-tailed Rayleigh model," *IEEE Transactions on Image Processing*, vol. 15, no. 9, pp. 2686–2693, 2006.

[4] F. Argenti, A. Lapini, T. Bianchi, and L. Alparone, "A tutorial on speckle reduction in synthetic aperture radar images," *IEEE Geoscience and Remote Sensing magazine*, vol. 1, no. 3, pp. 6–35, 2013.

[5] E. E. Kuruoglu and J. Zerubia, "Modeling SAR images with a generalization of the Rayleigh distribution," *IEEE Transactions on Image Processing*, vol. 13, no. 4, pp. 527–533, 2004.

[6] G. Moser, J. Zerubia, and S. B. Serpico, "SAR amplitude probability density function estimation based on a generalized Gaussian model," *IEEE Transactions on Image Processing*, vol. 15, no. 6, pp. 1429–1442, 2006.

[7] M. D. DeVore, A. D. Lanterman, and J. A. O'Sullivan, "ATR performance of a Rician model for SAR images," in *Automatic Target Recognition X*, vol. 4050. International Society for Optics and Photonics, 2000, pp. 34–45.

[8] J. Sun, X. Wang, X. Yuan, Q. Zhang, C. Guan, and A. V. Babanin, "The Dependence of Sea SAR Image Distribution Parameters on Surface Wave Characteristics," *Remote Sensing*, vol. 10, no. 11, p. 1843, 2018.

[9] M. Migliaccio, L. Huang, and A. Buono, "Sar speckle dependence on ocean surface wind field," *IEEE Transactions on Geoscience and Remote Sensing*, vol. 57, no. 8, pp. 5447–5455, 2019.

[10] S. Chitroub, A. Houacine, and B. Sansal, "Statistical characterisation and modelling of SAR images," *Signal Processing*, vol. 82, no. 1, pp. 69–92, 2002.

[11] S. Cui, G. Schwarz, and M. Datcu, "A comparative study of statistical models for multilook sar images," *IEEE Geoscience and Remote Sensing Letters*, vol. 11, no. 10, pp. 1752–1756, 2014.

[12] S. Ishii, S. Sayama, and K. Mizutani, "Effect of Changes in Sea-Surface State on Statistical Characteristics of Sea Clutter with X-band Radar," *Wireless Engineering and Technology*, vol. 2, pp. 175–183, 2011.

[13] J. R. M. Fernández, "Estimation of the relation between Weibull sea clutter and the CA-CFAR scale factor," *Revista Ingeniería*, vol. 25, no. 2, pp. 19–28, 2015.

[14] Z. Chen, X. Liu, Z. Wu, and X. Wang, "The Analysis of Sea Clutter Statistics Characteristics Based on the Observed Sea Clutter of Ku-Band Radar," in *2013 Proceedings of the International Symposium on Antennas & Propagation*, vol. 2. IEEE, 2013, pp. 1183–1186.

[15] X. Xing, Z. Chen, H. Zou, and S. Zhou, "Statistical assessment of model fit for SAR sea clutter," in *MIPPR 2009: Multispectral Image Acquisition and Processing*, vol. 7494. International Society for Optics and Photonics, 2009, p. 74940R.

[16] O. Karakuş, E. E. Kuruoğlu, and M. A. Altınkaya, "Generalized Bayesian model selection for speckle on remote sensing images," *IEEE Transactions on Image Processing*, vol. 28, no. 4, pp. 1748–1758, 2018.

[17] O. Karakuş, E. E. Kuruoğlu, and A. Achim, "Modelling sea clutter in SAR images using Laplace-Rician distribution," in *ICASSP 2020 - 2020 IEEE International Conference on Acoustics, Speech and Signal Processing (ICASSP)*, 2020, pp. 1454–1458.

[18] J.-M. Nicolas and F. Tupin, "A new parameterization for the Rician distribution," *IEEE Geoscience and Remote Sensing Letters*, 2019.

[19] T. Eltoft, "The Rician inverse Gaussian distribution: a new model for non-Rayleigh signal amplitude statistics," *IEEE Transactions on Image Processing*, vol. 14, no. 11, pp. 1722–1735, 2005.

[20] J. W. Goodman, "Statistical properties of laser speckle patterns," in *Laser speckle and related phenomena*. Springer, 1975, pp. 9–75.

[21] G. Gao, "Statistical modeling of SAR images: A survey," *Sensors*, vol. 10, no. 1, pp. 775–795, 2010.

[22] W. Wu, H. Guo, and X. Li, "Man-made target detection in urban areas based on a new azimuth stationarity extraction method," *IEEE Journal of Selected Topics in Applied Earth Observations and Remote Sensing*, vol. 6, no. 3, pp. 1138–1146, 2013.

[23] L. Denis, F. Tupin, and X. Rondeau, "Exact discrete minimization for TV+ L0 image decomposition models," in *2010 IEEE International Conference on Image Processing*. IEEE, 2010, pp. 2525–2528.

[24] R. A. Dana and D. L. Knepp, "The impact of strong scintillation on space based radar design ii: Noncoherent detection," *IEEE transactions on aerospace and electronic systems*, no. 1, pp. 34–46, 1986.

[25] H. A. Sturges, "The choice of a class interval," *Journal of the American Statistical Association*, vol. 21, no. 153, pp. 65–66, 1926.